Three-Dimensional Bioprinting and Electrospinning of Cellulose Nanocrystal/Polycaprolactone for Tracheal Scaffolds

Chen Feng,[a,c] Ji-ping Zhou,[b,*] Xiao-dong Xu,[a] Ya-ni Jiang,[b] Hong-can Shi,[d] and Guo-qi Zhao [c]

Three-dimensional printing (3DP) has high flexibility and controllability, and has attracted extensive attention in the biomedical field. However, the scaffolds prepared only by 3D bioprinting have poor mechanical properties, and they cannot effectively carry the required drugs. At the same time, compared with the size of cells, the pore size of 3D printed scaffolds is relatively large, and the efficiency of cell inoculation and tissue formation are still limited by the pore resolution of scaffolds. Therefore, a new method of forming 3D printing trachea composites is proposed. When combined, 3D bioprinting and electrospinning (ESP) can overcome the issues associated with scaffolds prepared by 3D bioprinting alone. Nanofibers create a suitable environment for cell growth. In terms of material use, Polycaprolactone (PCL) is commonly used as an ideal material source for 3D printing, but its biomechanical properties are insufficient. Cellulose nanocrystals (CNC) can effectively improve the properties of polymers such as PCL. Therefore, the inner layer of the scaffold used in tracheal surgery is created from PCL/CNC composite by 3D bioprinting, and the outer nano-cellulose film is deposited on the inner surface by electrospinning. Mechanical properties and cell adhesion/growth of scaffolds prepared by 3D bioprinting combined with electrospinning were found to be superior to those of scaffolds prepared by 3D bioprinting.

DOI: 10.15376/biores.17.4.6341-6357

Keywords: Three-dimensional printing; Electrospinning; PCL/CNC; Tracheal scaffold

*Contact information: a: Yangzhou Polytechnic Institute, Yangzhou 225127, China; b: College of Mechanical Engineering, Yangzhou University, Yangzhou 225009, China; c: College of Animal Science and Technology, Yangzhou University Yangzhou 225009, China; d: College of Medical, Yangzhou University, Yangzhou 225009, China; *Corresponding author: jpzhou@yzu.edu.cn*

INTRODUCTION

Accidental injuries, industrial accidents, cancer, idiopathic diseases, congenital anomalies, and medical diseases can damage trachea tissue (Li *et al*. 2017; Huang *et al*. 2021). In this context, rapid reconstruction of a patient's airway is important in clinical practice (Kennedy *et al*. 2021). When a trachea stenosis lesion occurs, the surgeon removes the diseased stenotic segment of the trachea and pulls down the remaining proximal and distal segments to secure the anastomosis. However, this procedure is not possible if the tracheal segment is ≥ 5 cm. Therefore, tissue engineering methods are needed (De Wit *et al*. 2021). Implantable decellularised tracheal matrices have been developed from human donor tissue to address the above problems. However, the number of cases treated in this way is limited, the cost is high, and the preparation of decellularised trachea matrix is time-

consuming (Li *et al*. 2017; Jung *et al*. 2020). In addition, post-implantation interventions such as multiple scaffold placements and bronchoscopy are required to prevent restenosis. Clinical use of tracheal scaffolds may be hampered by the long lead time resulting from the need for immediate airway replacement (Rowbotham *et al*. 2020; Tokunaga Kentaro *et al*. 2022). Also, decellularised tracheal matrices do not match the size and mechanical properties of individual patents' airways. Tissue-engineered scaffolds have good biocompatibility, biodegradability, and mechanical properties (Safari *et al*. 2022). Although various scaffolds have been developed with stem cells, they require *in vitro* preculture, *in vivo* ectopic implantation, and *in situ* transplantation, which hampers their widespread adoption. Regenerative therapy using a tracheal scaffold often fails because of restenosis (Huang *et al*. 2018; Lee *et al*. 2021). The trachea is a complex, multi-layered structure comprising a pseudo composite ciliated columnar epithelium, submucosa, a mature cartilage ring, and an outer membrane. Previous studies focused on structures that mimic cartilage regeneration of the trachea (Zang *et al*. 2012; Krishnan *et al*. 2020; Wang *et al*. 2021). However, without early regeneration of the inner respiratory epithelium, restenosis has resulted in failure of trachea tissue engineering.

3DP is a promising approach for engineering biomaterial scaffolds characterized by custom-shaped and fully interconnected networks of pores (Deshmane *et al*. 2021). It is often used in designing and fabricating hard tissue scaffolds such as bones (Griffin *et al*. 2020). 3D bio-printing has received much attention in the biomedical field in recent years due to its many potentially useful applications (Kelder *et al*.2018). It has obvious advantages of high flexibility and controllability which, compared with other traditional methods, are unparalleled. However, the scaffold prepared only through 3D bio-printing has a poor mechanical property, and it cannot effectively carry the required drug and provide a good micro-environment for cells' growth. Electrospinning technology and fused deposition molding technology based on 3D printing are of interest to the medical community (Yuan *et al*. 2022; Yang *et al*. 2020). Electrospinning is capable of producing submicron and nanoscale fibres. From a structural point of view, nanofibres are similar to the cytoplasmic matrix, and thus they can directly influence cellular behaviour. However, if only electrospinning is used, it is difficult to control the scaffold structure and the scaffold will have inadequate mechanical properties (Chen *et al*. 2011; Kumar *et al*. 2012). Therefore, combining 3D bioprinting extrusion with electrospinning to produce tissue-engineered scaffolds has been proposed. Martins *et al.* (2009) suggested scaffold fabrication by melt extrusion on a 3D printer, and that electrostatically spinning a nanofibre layer between the two layers of the scaffold structure could hamper bone scaffold production using only 3D printing or electrospinning. Centola *et al.* (2010) used electrospinning and fused deposition to produce a tissue-engineered vascular scaffold that did not induce endothelial differentiation or thrombosis. Liu *et al.* (2012) developed the 3D bioprinting composite moulding technique. After forming several macro scaffold structural layers, the electrospinning fibrous layers are compounded. This allows generation of internal pores and complex contours, ensuring excellent mechanical properties. Also, the micro- and nano-structures of the scaffold surface layer can be modified to optimise cell growth and adhesion. Liu *et al.* (2014) used a combination of electrospinning and 3D printing to control scaffolds with different pore architectures formed by fibre spacing. In this study, a combination of 3D printing extrusion and electrospinning was used to create a scaffold with the required mechanical properties and structure, which promoted cell growth adhesion, infiltration, and proliferation. This method can also be applied to methods such as nerve tissue engineering and bone tissue

regeneration. The composite moulding method employed in the present work holds much promise for tissue-defect repair.

EXPERIMENTAL

Test Materials and Instruments

The 3D printer used in the present study was Bio-Architect-Pro, which is manufactured by Hangzhou Regenovo Biotechnology Co., Ltd. (Hangzhou, China). The nanocellulose (CNC) was extracted from the stem of humulus (HJS), a kind of grass taken from the wild (Yangzhou, China). Polycaprolactone (PCL, relative molecular mass 120000, BR) was purchased from Shen Zhen Guanghua Weiye Co., Ltd. (Shenzhen, China). Dichloromethane (DCM, AR) and sulphuric acid (AR) were obtained from Tianjin Comeo Co., Ltd. (Tianjin, China).

Preparation of Cellulose Nanocrystals

Oxidised cellulose nanocrystals were obtained from HJS as follows:

(1) Grinding of HJS powder: HJS was washed with distilled water, dried in an oven for 12 h, crushed with a grinder, passed through a 40- to 60-mesh sieve, and dried in an oven for 4 h.

(2) Purification of plant fibres: Plant fibres were subjected to benzyl alcohol extraction, alkali treatment, and acid treatment to completely remove lignin and hemicellulose and obtain high-purity cellulose nanocrystals. HJS powder was dried, and 2 to 3 g was wrapped in filter paper and subjected to benzyl alcohol extraction in a clean Soxhlet extractor for 6 h. The powder was added to a constant-temperature (75 °C) shaking water bath. Lignin was removed by adding sodium chlorite solution (pH 5) and glacial acetic acid, and the powder was boiled in 4% sodium hydroxide with magnetic stirring for 2 h at 80 °C to remove hemicellulose.

(3) Collection of cellulose nanocrystals: purified HJS was added to sulphuric acid solution (mass fraction 60%) at a mass ratio of 1:1.15. The oxidation reaction was terminated by stirring and shaking in a water bath at 60 °C for 2 h and adding deionised water. Then centrifugate the obtained solution at a speed of 4000 r/min for 15 min to remove the supernatant. Centrifugation was repeated 3 to 4 times until no sediment was formed. The suspension was dialyzed with a dialysis bag for 48 h, with a change of the water every 24 h. The pH was cycled to reach 7, to obtain a cellulose nanocrystal suspension. Finally, the suspension was spray-dried, yielding CNC powder.

TEM of Cellulose Nanocrystals

The CNC solution was dropped onto the copper mesh for drying. The dried CNC particles were imaged with transmission electron microscope (TEM, Tecnai 12, Philips Co., Ltd., Amsterdam, Netherlands) using an acceleration voltage of 15 kV. The next step was to select 100 representative CNC particles in TEM photos and process them with image processing software image J (National Institute of health, USA) to calculate the diameter and length of nanocellulose.

Preparation of 3D-printing Biomaterials

Five equal masses of PCL particles were dissolved in a solvent of m(DMF):m(DCM) (30:70), left to stand at room temperature, dispersed in an ultrasonic bath (40 kHz) for 10 min, and mixed with CNC powder with magnetic stirring for 24 h. CNC powder was mixed with PCL (mass ratios 0, 1%, 3%, 5%, and 7%) and labelled CNC-X/PCL (where X = the amount of CNC added). The synthesised composites were poured into a mould (25 × 15 mm) preheated at 100 °C, placed in an oven for 18 h, and volatilised and dried at room temperature for 24 h to produce a film of approximately 0.8 mm thickness. CNC was used in amounts equivalent to approximately 0%, 1%, 3%, 5% and 7% of the mass of the PCL particles (Table 1).

Table 1. Chemical Compositions

Specimen	Specific Gravity of Dry CNC (%)	Weight of PCL (%)
PCL	0	100
CNC-1/PCL	1	99
CNC-3/PCL	3	97
CNC-5/PCL	5	95
CNC-7/PCL	7	93

Characterisation of CNC/PCL

Infrared spectroscopy

Fourier transform infrared spectroscopy (FTIR, 670-ir 670-ir+610-ir, Varian Co., Ltd., Palo Alto, CA, USA) was used to test the functional group changes of the samples. The scanning range is 400 to 4000 cm^{-1}, and the resolution is 4 cm^{-1}.

DSC

Differential scanning calorimetry (DSC) was performed using a DSC 2010 TA instrument (Newcastle, DE, USA). Samples were heated from −10 °C to 200 °C with a 10 °C/min heating rate under 25 mL/min nitrogen atmosphere. Samples were kept for 5 min at 200 °C to remove thermal memory. Samples were then cooled to 0 °C with 10 °C/min cooling rate.

X-ray diffraction (XRD)

X-ray diffractometry was used to evaluate the effect of CNC on PCL crystals. The test was carried out in reflection mode with a scanning angle of 5 to 40° (2θ), and the crystallinity of the fibre structure was examined at a rate of 2°/min. The relative crystallinity of CNC was calculated by the following Eq. 1 (Nolin *et al*. 2022):

$$C_r = [A_c \div A_a] \times 100\% \quad (1)$$

where A_a and C_r are the total peak area covering the amorphous diffraction peak and relative crystallinity, respectively, and A_c is the sum of the areas of the crystalline diffraction peaks.

Cell culture and seeding

All animal surgeries and handling were performed in accordance with the "Guide for the Care and Use of Laboratory Animals" Eighth Edition formulated by the National Academy of Sciences Act of 2011 following ethical approval from the Ethics Committee of Medical College of Yangzhou University.

At present, the most commonly used marrow derived mesenchymal stem cells (MSCs) are murine cells. In separate work, SPF grade 3-to 4-week old SD rats were killed by neck amputation and soaked in 75% alcohol for 5 min. Under sterile conditions, the bilateral femurs of rats were separated, and the muscle tissue attached to them was completely removed. The epiphysis at both ends was removed. The bone marrow cavity was repeatedly rinsed with l-dmem mesenchymal stem cell culture medium containing 10% fetal bovine serum. The cells were collected, centrifuged at 1100 r/min for 5 min, and the supernatant and fat layer were discarded. Then, it was inoculated into culture flasks at a density of 2×10^5 cells/cm^2 and cultured in an incubator. After 48 hours of culture, the solution was changed for the first time, and then every 3 days. The morphology and growth of cells were observed every day. 3DP scaffolds, both with and without ESP collagen film, were cut into 1×1 cm^2 sheets and washed twice in the PBS. The MSCs were resuspended in culture medium at 1×10^6 /mL and uniformly seeded onto these scaffolds; 10 mL of culture medium was gently added after the scaffolds were placed in a 37 °C incubator for 4 h. The medium was replaced every 2 days. The incubation of the cell-loaded scaffolds depended on further cellular experiments.

Apoptosis assay

The Hoechst 33342/propidium iodide (PI) double staining method was used to stain nuclei of normal and apoptotic cells. MSCs were incubated in 24-well plates for 48 h in impregnation medium, washed twice in phosphate-buffered saline (PBS) (pH 7.4), and stained with Hoechst 33342 (10 ng/mL) and PI (10 ng/mL) for 20 min at 4°C, while being protected from light.

Preparation of Tracheal Scaffolds

A novel bilayer tubular scaffold was fabricated as an artificial trachea, consisting of a fibrous membrane of electrospun composites (outer layer) and a 3D bioprinted scaffold (inner layer). By inoculating mesenchymal stem cells (MSCs) into the outer layer, the tissue-engineered trachea was epithelialised and chondrogenic, preventing scaffold collapse (Wang *et al*. 2019). The epithelial cells not only remove secretions and inhaled particles, but they also activate and adsorb inflammatory cells. The outer nanofibre structure acts as a mucosal layer, facilitating cell growth (Fig. 1). The inner layer provides mechanical strength and elasticity, acting as a framework for the trachea. MSCs in the inner and outer layers promote regeneration of cartilage and epithelial tissue (Smith *et al*. 2020; He *et al*. 2021).

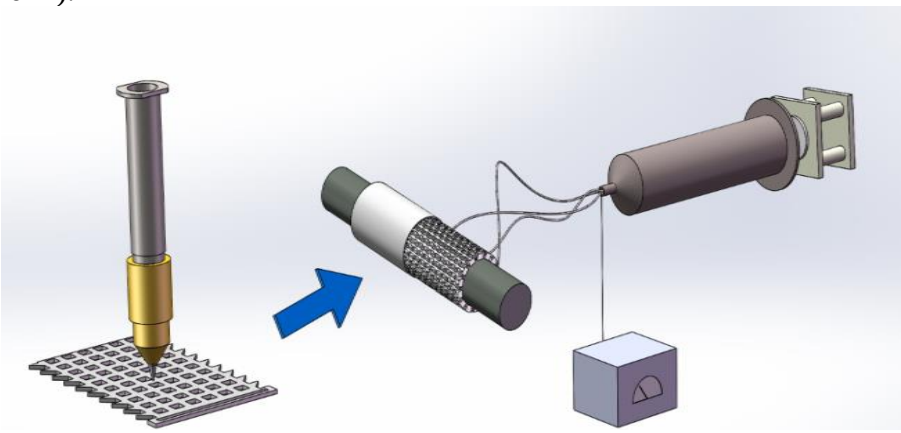

Fig. 1. Schematic of the combination of 3D printing and electrospinning

Three-dimensional printing of the scaffold inner layer

The inner layer of the tracheal scaffold provides mechanical support, and the flat scaffold could be rolled into a cylinder. According to the characteristics of the tracheal scaffold and the different diameters required by different tracheas, a sliding button type tracheal scaffold was designed. A layer of outer frame was printed on the leftmost end of the scaffold to clamp the sliding teeth, and a layer of sliding teeth was printed on the upper and lower ends of the stent to be fixed through the outer frame. After printing, the tail end of the scaffold was curled through the outer frame of the scaffold. According to the needs of different tracheal diameters, cylindrical scaffold structures of various sizes can be formed. The thickness of the bracket is generally printed as 0.3 to 0.4 mm, and the structure of the slide button type tracheal bracket is shown in Fig. 2. This structure not only is able to avoid the loss of mechanical properties caused by plastic deformation of polymer materials, but also it can reduce the acute elastic retraction of scaffolds in theory. The scaffold inner layer was prepared as follows. A computer was used to create a concave hexagonal filling model. The flat scaffold was rolled (Fig. 3), and a suitable forming path was generated. CNC/PCL composites with good mechanical properties were selected. A slip-fastened planar scaffold 3D was bioprinted in a layer-by-layer manner (Fig. 4a) to prepare a trachea with a concave hexagonal pore structure for the cylindrical tube wall. The scaffold was autoclaved and prepared as shown in Fig. 4b.

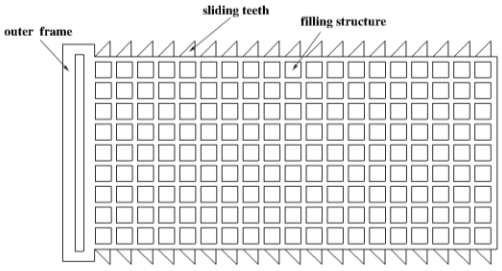

Fig. 2. Structure of a sliding pipe scaffold

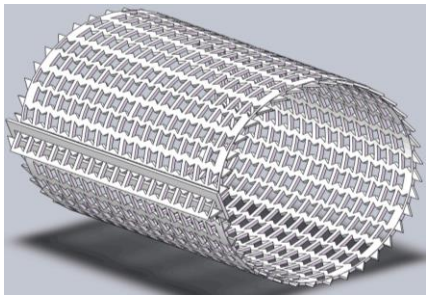

Fig. 3. Model of the concave hexagonal porous trachea scaffold

(a) **(b)**

Fig. 4. (a) Concave hexagonal printed scaffold; (b) cylindrical trachea scaffold

Electrospinning liquid

PCL pellets were dissolved in m (DMF):m(DCM) (30:70) at a mass fraction of 8%. Lyophilised CNC was added to the PCL solution and stirred continuously at room temperature for 48 h. Similarly, CNC was loaded at 0%, 1%, 3%, and 5% of the mass of PCL.

Fabrication of scaffold outer layers by electrospinning

The CNC-3/PCL solution was injected into a 5 mL (23 G, 0.5") syringe and electrospun on a rotating stainless-steel mandrel (diameter 20 mm) with 30 cm separating the needle tip and rotating collector. The voltage applied to the needle was 7 kV and the negative high voltage was 3 kV. The push rate was 0.6 mL/h. A metal rod receiver 20 mm in diameter was used, with a rotation time of 8 h. Tubular nanofibres (scaffold outer layer; length = 100 mm, thickness = ~30 μm) were prepared on the surface of the rotating mandrel. The CNC/PCL nanofibres were dried overnight in a vacuum oven (40 °C) to eliminate residual solvents (Fig. 5).

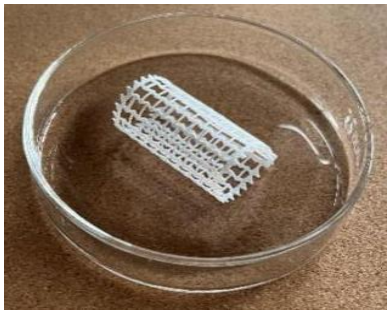

Fig. 5. Preparation of the outer layer by electrospinning

Scaffold Performance Testing

Mechanical properties

The compressive and tensile strength were evaluated using a self-developed automatic tensile tester. The tracheal scaffold formed by 3D printing and electrospinning is marked as scaffold I, and the scaffold produced by 3D printing only is marked as scaffold II. Both printing methods used CNC-3/PCL composite materials. The scaffold tensile strength refers to the resistance of the scaffold to longitudinal external compression, and the compressive strength reflects the maximum resistance in the transverse direction. Ten specimens of each of two types of scaffolds were prepared, and mean values were calculated. For tensile strength testing, each specimen was placed on both ends of the fixture and tested at a constant speed of 0.1 mm/s at room temperature until the material was pulled. For the scaffold, the tensile mechanism was replaced with an upper platen mechanism and the specimen was placed in the centre of the lower platen. An initial load of 0.1 N was applied at 0.1 mm/s at room temperature. The load force was recorded when the tube diameter was compressed to 50%.

Scanning electron microscopy (SEM)

Scaffold microstructure was assessed using a scanning electron microscope (S-4800; Hitachi, Tokyo, Japan). Specimens were frozen in liquid nitrogen. Two jigs were used to expose the cross-section before observation.

Biocompatibility testing

The 3D-printed scaffold, biocomposite scaffold, and control were soaked in PBS containing double antibodies for 1 h, UV-irradiated for 1 h, and incubated in a water bath at 70 °C for 1 h. Next, 3 mL of complete culture medium was added and incubated at 37 °C for 24 h. Based on their ability to differentiate into multiple lineages, MSCs (2.5×10^3 per well) were incubated in 96-well plates in a CO_2 incubator for 5 days. The optical

density (OD) at 450 nm was measured by enzyme-linked immunoassay on days 1, 3, and 5. Finally, MSC morphology was visualised by field-emission scanning electron microscopy.

RESULTS AND DISCUSSION

CNC Characterisation

In the field of composites, when CNC is used as reinforcement, a high aspect ratio will be more conducive to improve the mechanical properties of composites. Therefore, a high aspect ratio is an important index to measure the properties of nano cellulose. According to the TEM photos separated from HJS, the average length of CNC was 359.68 ± 98.46 nm, the average diameter was 11.24 ± 5.11nm, and the average aspect ratio was 32.00 ± 10.8. Therefore, CNC separated from HJS had good application value (Fig. 6).

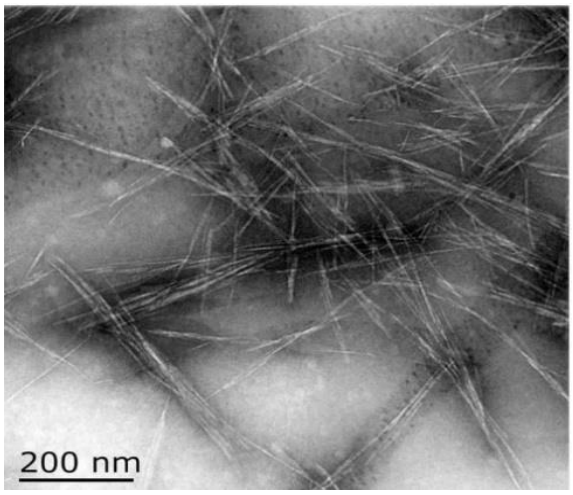

Fig. 6. TEM image of CNCs

Fourier-Transform Infrared (FTIR) Analysis

FTIR analysis was used to study PCL- and CNC/PCL-reinforced nanofiber composites (Fig. 7). As the CNC content of PCL increased, the peak at around 3300 cm^{-1} (telescopic vibrational peak of O-H groups (Alemdar and Sain 2008) increased in size. The strong absorbance peaks at 3000 to 2850 cm^{-1} corresponded to C-H bond stretching vibrations (Sun *et al*. 2011). The absorbance peak of C=O stretching vibrations was located at 1731 cm^{-1}. Bands in the range 1500 to 1250 cm^{-1} are affected by the C-H bending vibrations (CH_2 bending rings at 1468 and 1365 cm^{-1}, and C-C and C-O stretching at 1294 cm^{-1}). The absorbance peaks at 1057 and 1170 cm^{-1} represent the C-H stretching vibration absorption peak of the glycosidic bond and cellulose C-O stretching vibration, respectively.

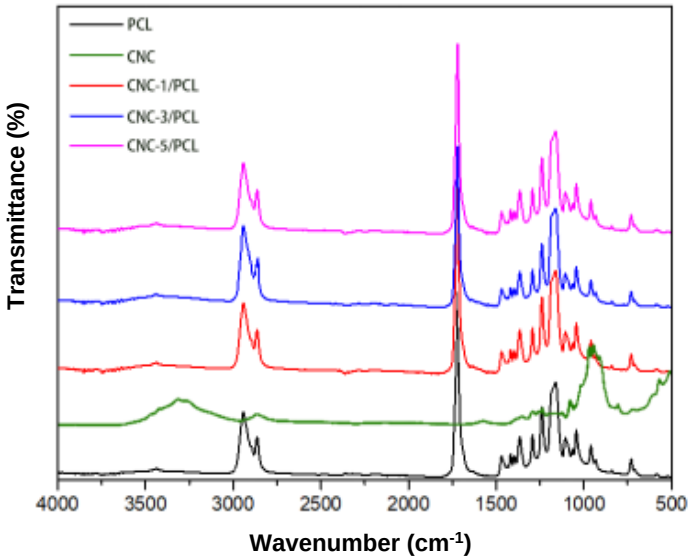

Fig. 7. FTIR analysis of CNC/PCL

There is a close association between the peak at 750 cm^{-1} and O-H stretching vibration, while the main vibrational absorption peaks of PCL without the addition of CNC are those of CH_2 and C=O. The increase in intensity of the hydroxyl absorption peak with increasing CNC content was not significant, particularly at 3%. The absence of new absorption peaks on composites also indicates that CNC and PCL were physically mixed, and that CNC had been successfully incorporated into the PCL nanofibres.

Thermal Stability

The thermal stabilities of CNC/PCL composites were investigated by DSC (Fig. 8). The material melting temperature (T_m) and enthalpy of melting (ΔH_m) are shown in Table 2. ΔH_m reflects the melting heat and, indirectly, the crystallinity of the material. CNC led to more efficient PCL crystallisation at higher temperatures. This suggests that CNC acts as a nucleating agent for the crystallisation of PCL (Voronova *et al*. 2022). The melting enthalpy of composites showed a trend of increasing and then decreasing as the loading of CNC increased, similar to the trend of crystallinity. This shows that trace amounts of CNC within the PCL can be used as a nucleating agent. The DSC curves for pure PCL materials are consistent with the trends of CNC-1/PCL, CNC-3/PCL and CNC-5/PCL composites. Thus, there was only a physical reaction between CNC and PCL; no chemical reaction took place. Therefore, no additional energy was needed to break the chemical bonds between them.

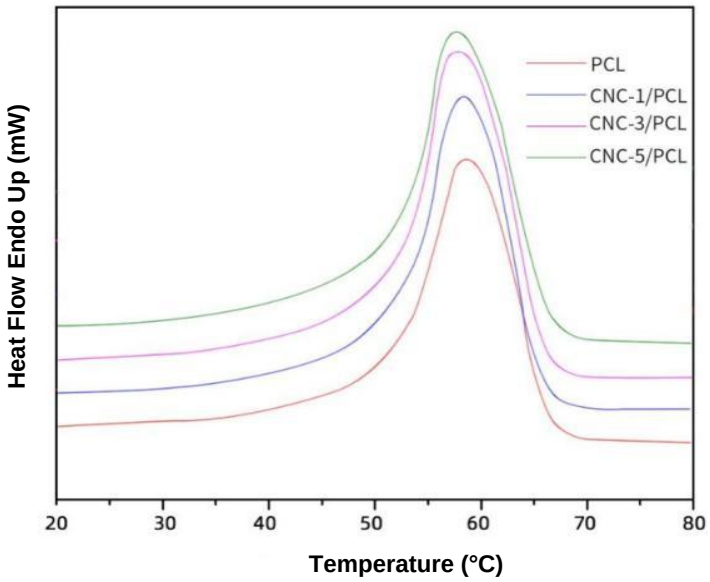

Fig. 8. DSC analysis of pure PCL and CNC/PCL nanocomposites

Table 2. T_m and ΔH_m Values

Specimen	T_m (°C)	ΔH_m (J.g^{-1})
PCL	58.92	54.2415
CNC-1/PCL	58.51	55.7982
CNC-3/PCL	58.23	56.2901
CNC-5/PCL	57.89	54.8577

Crystallinity

The results of XRD analysis of the crystalline structure of cellulose are shown in Table 3, and the crystal structures are illustrated in Fig. 9. The diffraction intensity of CNC was weaker than that of PCL. The crystal azimuth of PCL and its composites was almost in the same direction. PCL showed two peaks (near 22° and 24°) at 2θ. The crystalline diffraction intensities of the composites at the two main diffraction peaks (110) and (200) were higher than those of pure PCL, indicating the formation of a semi-crystalline polymer during preparation (Agarwal *et al*. 2010; Hivechi *et al*. 2018; Rashtchian *et al*. 2020). The crystallinity of the composites increased with CNC content up to 5%, and it tended to decrease at higher CNC contents. This was because a small amount of CNC promoted the nucleation of PCL, thereby increasing crystallinity. When present in larger amounts, CNC agglomerates, which prevents an orderly arrangement of PCL and restricts the movement of PCL chains (Prado and Spinacé 2019), thus decreasing composite crystallinity. The H_m and X_c values increased and then decreased with the addition of increasing amounts of CNC (Table 3).

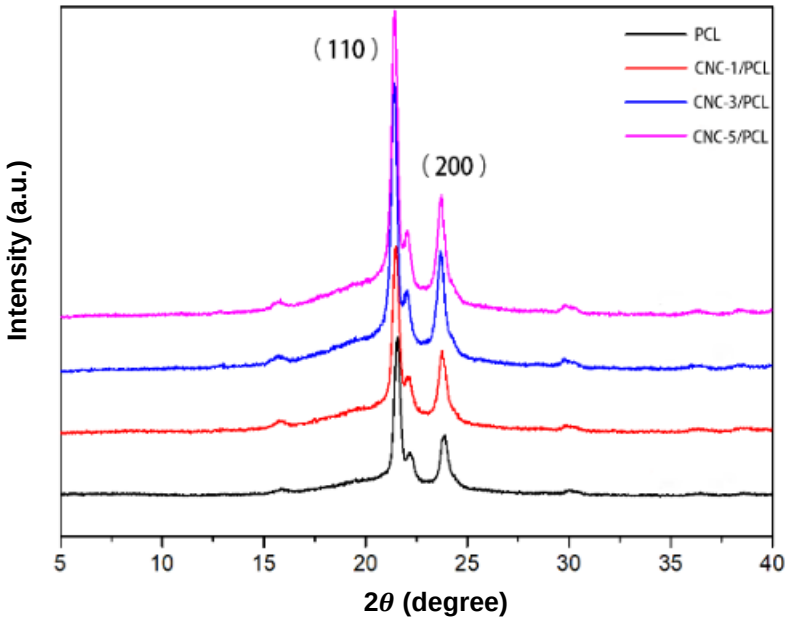

Fig. 9. XRD analyses of pure PCL and CNC/PCL

Table 3. Crystallinity of PCL and CNC/PCL Composites

Specimen	Crystallinity X_c (%)
PCL	63.58
CNC-1/PCL	65.77
CNC-3/PCL	71.39
CNC-5/PCL	70.78

Apoptosis

The PCL, CNC-3/PCL, and control groups had large numbers of live cells and few dead cells, indicating good biocompatibility (Fig. 10). The apoptosis rate was approximately 3.91 ± 0.03% in the PCL group, 3.98 ± 0.04% in the CNC-3/PCL group, and 2.27 ± 0.03% in the control group; there was no significant group difference.

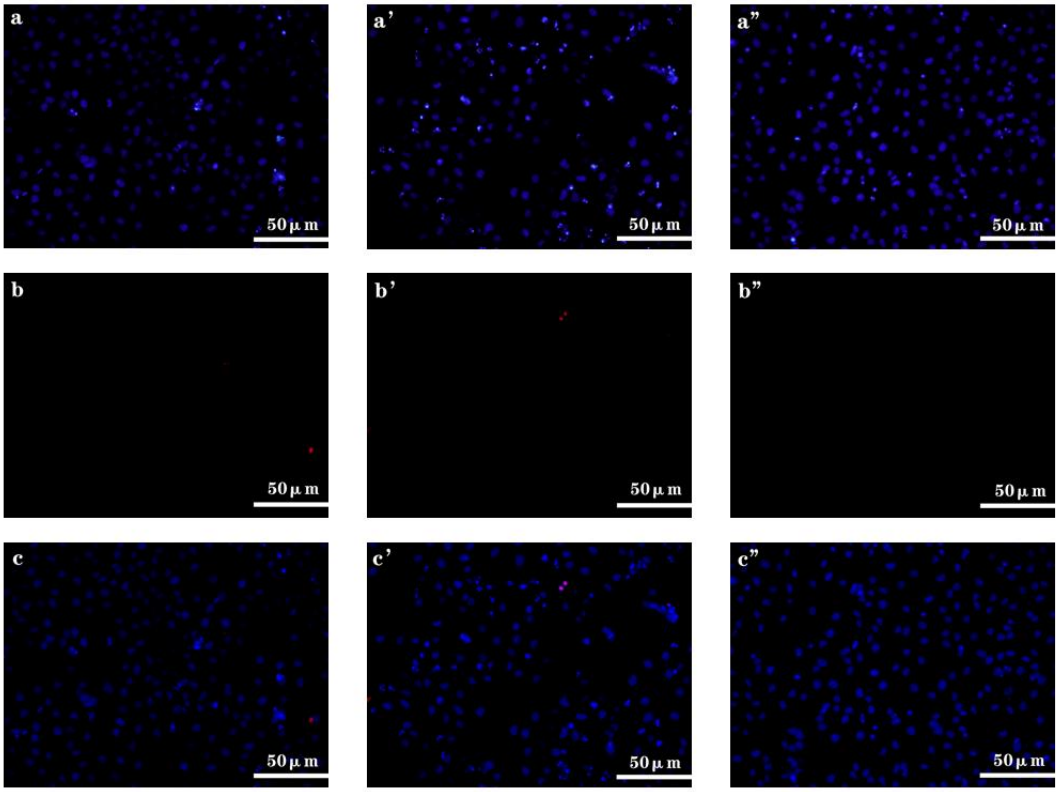

Fig. 10. Live(a，a'，a'') and dead cells (b，b'，b'') in the PCL group (a, b, c), CNC-3/PCL group (a', b', c') and control group (a'', b'', c'')

Mechanical Properties

Under the same biological composite material, the mechanical properties of the Scaffold I with electrospinning and 3D printing technology were compared with that of the Scaffold II with 3D printing technology only. The tensile strength (maximum stress until fracture (Han *et al*. 2013)) of type I and II scaffolds was 19.5 ± 1.2 and 17.8 ± 1.5 MPa, respectively (Table 4). The radial strength of type I and II scaffolds was 128 ± 11.8 and 121 ± 12.9 kPa, respectively. Therefore, it can be judged that the radial strength of both types of scaffold is sufficient for clinical use (typical requirement, 80 to 120 kPa) (Table 4).

Table 4. Mechanical Properties of the Tracheal Scaffolds

Parameter	Scaffold I	Scaffold II
Thickness (mm)	0.404	0.410
Tensile strength (MPa)	19.5±1.2	17.8±1.5
Radial strength (kPa)	128±11.8	121±12.9

SEM Analysis

The scaffold outer layer consisted of uniformly distributed high-quality CNC/PCL fibres of uniform diameter, which were suitable for cell growth (Fig. 11). The composite scaffold consisted of a two-layer structure, with an inner layer approximately 0.4 mm thick

(measured using a micrometre; accuracy = ± 0.01 mm) and an outer layer approximately 0.05 mm thick (Fig. 10).

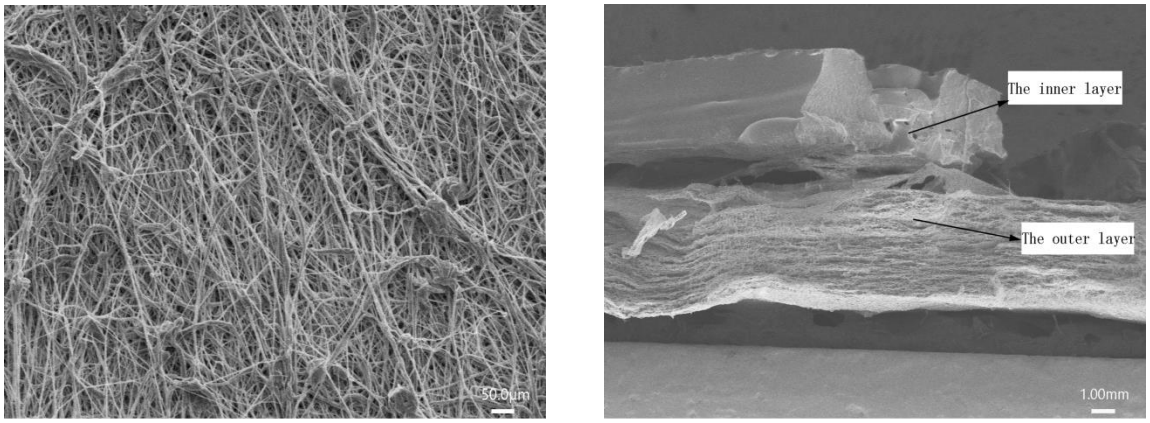

Fig. 11. SEM of the outer layer of the tracheal scaffold and cross-sections of the inner and outer layers of the tracheal scaffold

Scaffold Biocompatibility

The absorbance values of all wells increased over time (Fig. 12), indicating active cell proliferation on the scaffolds. One-way ANOVA showed that cells on the electrospinning combined with 3D printing scaffold proliferated more rapidly than those on the 3D-printed scaffold ($p < 0.05$), and that the proliferation rate on the former increased with time. Therefore, the novel tracheal scaffold had good biocompatibility.

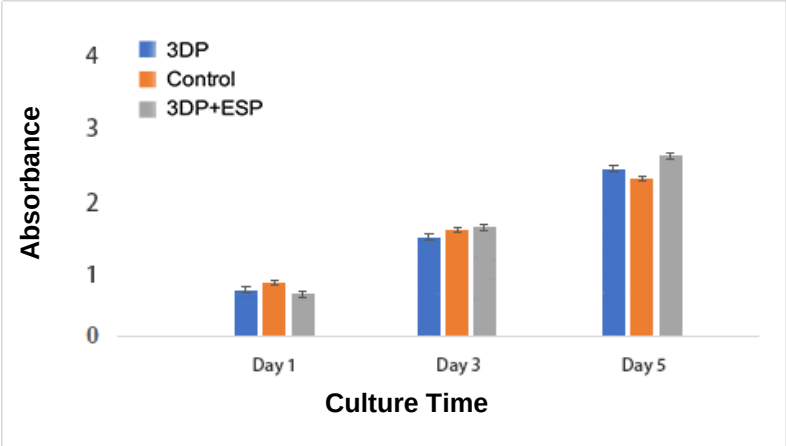

Fig. 12. Scaffold cytotoxicity

CONCLUSIONS

1. The cellulose nanocrystals (CNCs) were isolated from humulus stem (HJS) by sulfuric acid hydrolysis. The CNC was used as nano reinforcement to prepare CNC/poly(capro lactone) (PCL) composite biomaterials for biological 3D printing trachea scaffold. The average length of CNC was about 360 nm, the average diameter was approximately 11.2 nm, and the average aspect ratio was about 32. Its high aspect ratio and crystallinity make it an excellent choice for composite reinforcement.

2. PCL/CNC physical properties, thermal properties, crystallization behavior and biocompatibility were evaluated. It was found that CNC effectively acted as a nucleating agent. The higher the CNC content, the higher the pore density, which can play an enhancing role. The solid samples with higher CNC content exhibited better mechanical properties, which reached the maximum at 5% CNC content. The crystallinity was maximized when the content reached 3%. In addition, the biocompatibility of CNC/PCL nanocomposites was tested by culturing mesenchymal stem cells (MSCs). The results showed that the nanocomposites were suitable for cell growth and CNC helped to improve the biocompatibility of nanocomposites.
3. This study presents a novel method of creating tracheal scaffolds with enhanced mechanical properties and cell adsorption. The surface of the scaffold is covered by an electrospun fibre membrane. The mechanical properties and stability of the new tracheal scaffold were superior to those of a 3D-printed tracheal scaffold. These findings indicated that biological composites can be promising biomaterials for injury-repair of tracheal injury and a hybrid process (an electrospinning based rapid-prototyping method) to fabricate biological composite scaffolds. These can be an improvement relative to conventional 3D printing technology and provide new possibilities.

ACKNOWLEDGMENTS

This work was supported financially by the National Natural Science Foundation of China (No. 81770018) and Yangzhou-Yangzhou Polytechnic Institute Project (No.2021xjzk018) and The Natural Science Foundation of the Jiangsu Higher Education Institutions of China (No. 22KJD460011).

REFERENCES CITED

Alemdar, A., and Sain, M. (2008). "Isolation and characterization of nanofibers from agricultural residues: Wheat straw and soy hulls," *Bioresource Technology* 99(6), 1664-1671. DOI: 10.1016/j.biortech.2007.04.029

Centola, M., Rainer, A., and Spadaccio, C. (2010). "Combining electrospinning and fused deposition modeling for the fabrication of a hybrid vascular graft," *Biofabrication* 2(1), 1067-1075. DOI: 10.1088/1758-5082/2/1/014102

Chen, H.-K., Zhang, J.-L., Wu, H.-P., Li, Y.-J., Li, X., Zhang, J.-X., Huang, L.-H., Deng, S.-P., Tan, S.-Z., and Cai, X. (2021). "Fabrication of a Cu nanoparticles/poly(ε-caprolactone)/gelatin fiber membrane with good antibacterial activity and mechanical property via green electrospinning," *ACS Appl Bio Mater* 4, 6137-6147. DOI: 10.1021/acsabm.1c00485

Deshmane, S., Kendre, P., Mahajan, H., and Jain, S. (2021). "Stereolithography 3D printing technology in pharmaceuticals: A review," *Drug Dev. Ind. Pharm.* 47(9), 1-11. DOI: 10.1080/03639045.2021.1994990

De Wit, R., Siddiqi, S., Tiemessen, D., Snabel, R., Veenstra, G. J., Oosterwijk, E., and Verhagen, A. (2021). "Isolation of multipotent progenitor cells from pleura and pericardium for tracheal tissue engineering purposes," *J. Cell. Mol. Med.* 25(23),

10869-10878. DOI: 10.1111/jcmm.16916

Griffin, M., Castro, N., Bas, O., Saifzadeh, S., Butler, P., and Hutmacher, D. W. (2020). "The current versatility of polyurethane three-dimensional printing for biomedical applications," *Tissue Eng. Part B Rev.* 26(3), 272-283, DOI: 10.1089/ ten.TEB.2019.0224

Han, F.-X., Jia, X.-L., Dai, D.-D., Yang, X.-L., Zhao, J., Zhao, Y.-H., Fan, Y.-B., and Yuan, X.-Y. (2013). "Performance of a multilayered small-diameter vascular scaffold dual-loaded with VEGF and PDGF," *Biomaterials* 34(30), 7302-7313. DOI: 10.1016/j.biomaterials.2013.06.006

He, X.-Y., Yu, H.-M., Lin, S., and Li, Y.-Z. (2021). "Advances in the application of mesenchymal stem cells, exosomes, biomimetic materials, and 3D printing in osteoporosis treatment," *Cell. Mol. Biol. Lett.* 26, 47. DOI: 10.1186/s11658-021-00291-8

Hivechi, A., Bahrami, S. H., and Siegel, R. A. (2018). "Drug release and biodegradability of electrospun cellulose nanocrystal reinforced polycaprolactone," *Mater. Sci. Eng. C Mater. Biol. Appl*. 94, 929-937. DOI: 10.1016/j.msec.2018.10.037

Huang, J.-T., Zhang, Z,-W., and Zhang, T. (2018). "Suture fixation of tracheal scaffolds for the treatment of upper trachea stenosis: A retrospective study," *J. Cardiothorac. Surg.* 13(1), 111. DOI: 10.1186 /s13019-018-0790-x

Huang, Z.-J., Wei, P., Gan, L.-M., Li, W.-T., Zeng, T.-H., Qin, C.-C., Chen, Z.-Y., and Liu, G.-N. (2021). "Protective effects of different anti-inflammatory drugs on tracheal stenosis following injury and potential mechanisms," *Mol. Med. Rep*. 23(5). DOI: 10.3892/mmr.2021.11953

Jung, S. Y., Tran, A. N.-T., Kim, H. Y., Choi, E., Lee., S. J., and Kim, H. S. (2020). "Development of acellular respiratory mucosal matrix using porcine tracheal mucosa," *Tissue Eng. Regen. Med*. 17(4), 433-443. DOI: 10.1007/s13770-020-00260-w

Kelder, C., Bakker, A. D., Klein-Nulend, J., and Wismeijer, D. (2018). "The 3D printing of calcium phosphate with K-carrageenan under conditions permitting the incorporation of biological components-A method," *J. Funct. Biomater.* 9(4). DOI: 10.3390/jfb9040057

Kennedy, A. A., de Alarcon, A., Tabangin, M. E., Rutter, M. J., Myer, C. M., Smith, M. M., and Hart, C. K. (2021). "Tracheal A-frame deformities following airway reconstruction," *Laryngoscope* 131(4), E1363-E1368. DOI: 10.1002/lary.28996

Krishnan, U., Singh, H., Tedla, N., Leach, S. T., and Kaakoush, N. O. (2020). "Presence of gastric pepsinogen in the trachea is associated with altered inflammation and microbial composition," *Infect. Immun*. 88(12). DOI: 10.1128/IAI.00455-20

Kumar, G., Waters, M., and Farooque, T. (2012). "Freeform fabricated scaffolds with roughened struts that enhance. Both stem cell proliferation and differentiation by controlling cell shape," *Biomaterials* 33, 4022-4030. DOI: 10.1016/j.biomaterials.2012.02.048

Lee, T.-G., Jang, S. J., and Choi, S. H. (2021). "Intraluminal titanium alloy scaffold to prevent tracheal stenosis in tracheal anastomosis," *in Vivo* 35(6), 3175-3180. DOI: 10.21873/invivo.12612.

Li, L. H., Xu, M. P., Gan, L. M., Li, Y., Liang, Y. L., Li, W. T., Qin, E. Y., Gan, J. H., and Liu, G. N. (2017). "Effect of low dose erythromycin on the proliferation of granulation tissue after tracheal injury," *Zhonghua Yi Xue Za Zhi* 97(10), 777-781. DOI: 10.3760/cma.j.issn.0376-2491.2017.10.012

Li, P., Li, S.-S., Tang, Q.-L., He, X.-B., Yin, D.-H., Wang, S., and Yang, X.-M. (2017). "Reconstruction of human oncological tracheal defects with xenogenic acellular dermal matrix," *Auris Nasus Larynx* 44(2), 237-240, DOI: 10.1016/j. anl.2016.04.008.

Liu, Y.-y., Zhang, F.-h., Chen, W.-h., Yan, F.-f., Zheng, L.-l., and Hu., Q.-x. (2014). "CAD/CAM system and experimental study of biological 3D printing composite process," *Journal of Mechanical Engineering* 50(15), 147-154. DOI: 10.3901/JME.2014.15.147

Liu, D.-l., Liu, Y.-y., Wang, Q.-g., Jing, C. and Hu, Q. (2012). "Multiphysics coupling analysis and experiment of low-temperature deposition manufacturing and electrospinning for multi-scale tissue engineering scaffold," *Journal of Mechanical Engineering* 48(15), 137-143. DOI:10.3901/JME.2012.15.137

Martins, A., Chung, S.-W., Pedro, A. J., Sousa, R. A., Marques, A. P., Reis, R. I., and Neves, N. M. (2009). "Hierarchical starch-based fibrous scaffold for bone tissue engineering applications," *Journal of Tissue Engineering and Regenerative Medicine* 3(1), 37-42. DOI: 10.1002/term.132

Mondal, K., Bhagabati, P., Goud, V. V., Sakurai, S., and Katiyar, V. (2021). "Utilization of microalgae residue and isolated cellulose nanocrystals: A study on crystallization kinetics of poly(ε-caprolactone) bio-composites," *Int. J. Biol. Macromol*. 191, 521-530. DOI: 10.1016/j.ijbiomac.2021.09.114

Nolin, A., Pierson, K., Hlibok, R., Lo, C.Y., Kayser, L. V., and Dhong, C.(2022). "Controlling fine touch sensations with polymer tacticity and crystallinity," *Soft Matter*, 18(20), 3928-3940. DOI:10.1039/d2sm00264g

Prado, K. S., and Spinacé, M. A. S. (2019). "Isolation and characterization of cellulose nanocrystals from pineapple crown waste and their potential uses," *Int. J. Biol. Macromol.* 122, 410-416. DOI: 10.1016/j.ijbiomac.2018.10.187

Rashtchian, M., Hivechi, A., Bahrami, S. H, Milan, P. B., and Simorgh, S. (2020). "Fabricating alginate/poly(caprolactone) nanofibers with enhanced bio-mechanical properties *via* cellulose nanocrystal incorporation," *Carbohydr. Polym.* 233, article no. 115873. DOI: 10.1016/j.carbpol.2020.115873

Rowbotham, N. J., Smith, S. J., Davies, G., Daniels, T., Elliott, Z. C., Gathercole, K., Rayner, O. C., and Smythe, A. R. (2020). "Can exercise replace airway clearance techniques in cystic fibrosis? A survey of patients and healthcare professionals," *J. Cyst. Fibros.* 19(4), e19-e24. DOI: 10.1016/j.jcf.2019.10.026

Safari, B., Aghanejad, A., Kadkhoda, J., Aghazade, M., Roshangar, L., and Davaran, S. (2022). "Biofunctional phosphorylated magnetic scaffold for bone tissue engineering," *Colloids Surf B Biointerfaces* 211, article no. 112284. DOI: 10.1016/j .colsurfb.2021.112284.

Smith, B. T., Bittner, S. M., Watson, E., Smoak, M. M., Diaz-Gomez, L., Molina, E. R., Kim, Y. S., Hudgins, C. D., Melchiorri, A. J., Scott, D. W., *et al.* (2020). "Multimaterial dual gradient three-dimensional printing for osteogenic differentiation and spatial segregation," *Tissue Eng. Part A* 26, 239-252. DOI: 10.1089/ten.TEA.2019.0204

Sun, K.-J., Zhang, J.-T., Cehn, Y., Liao, Z.-W., Lin, R., and Cong, L. (2011). "Accelerating the degradation of green plant waste with chemical decomposition agents," *J Environ Manage* 92, 2708-2713. DOI: 10.1016/j.jenvman.2011.06.011.

Tokunaga, K., Ejima, T., Nakashima, T., Kuwahara, M., Narimatsu, N., Sagishima, K., Mizumoto, T., Sakagami, T., and Yamamoto, T. (2022) "A novel technique for

assessment of post-extubation airway obstruction can successfully replace the conventional cuff leak test: A pilot study," *BMC Anesthesiol.* 22(1), 38, DOI: 10.1186/s12871-022-01576-x

Voronova, M. I., Gurina, D. L., and Surov, O. V. (2022). "Co-properties of poly(3-hydroxybutyrate—3-hydroxyvalerate)/polycaprolactone polymer mixtures reinforced by cellulose nanocrystals: Experimental and simulation studies," *Polymers (Basel)* 14. DOI: 10.3390/polym14020340

Wang, J.-Q., Jiang, B.-J., Guo, W.-J., and Zhao, Y.-M. (2019). "Indirect 3D printing technology for the fabrication of customized β-TCP/chitosan scaffold with the shape of rabbit radial head-An *in vitro* study," *J. Orthop. Surg. Res.* 14, 102. DOI: 10.1186/s13018-019-1136-7

Wang, Z.-H., Sun, F., Lu, Y., Zhang, B.-Y., Zahng, G.-Z., and Shi, H.-C. (2021). "Rapid preparation method for preparing tracheal decellularized scaffolds: Vacuum assistance and optimization of DNase I," *ACS Omega* 6(16), 10637-10644. DOI: 10.1021/acsomega.0c06247

Yang, Z., Song, Z.-C., Nie, X., Guo, K.-J., and Gu, Y. (2020). "A smart scaffold composed of three-dimensional printing and electrospinning techniques and its application in rat abdominal wall defects," *Stem Cell Res. Ther.* 11(1), 533. DOI: 10.1186/s13287-020-02042-6

Yuan, Z.-C., Ren, Y.-J., Shafiq, M., Chen, Y.-J., Tang, H., Li, B.-J., EL-Newehy, M., EL-Hamshary, H., Morsi, Y., Zheng, H., and Mo, X.-M. (2022). "Converging 3D printing and electrospinning: Effect of poly(l-lactide)/gelatin based short nanofibers aerogels on tracheal regeneration," *Macromol. Biosci*. 22(1), article no. e2100342. DOI: 10.1002/mabi.202100342

Zang, M.-Q., Zhang, Q.-X., Chang, E. I., Mathur, A. B., and Yu, P.-R. (2012). "Decellularized tracheal matrix scaffold for tissue engineering," *Plast. Reconstr. Surg.* 130(3), 532-540. DOI: 10.1097/PRS.0b013e31825dc084

Article submitted: July 14, 2022; Peer review completed: September 11, 2022; Revised version received: September 18, 2022; Accepted; September 19, 2022; Published: September 27, 2022.
DOI: 10.15376/biores.17.4.6341-6357